Threshold production of unstable top

Alexander A. Penin

Department of Physics, University of Alberta,
Edmonton AB T6G 2J1, Canada
Institut für Theoretische Teilchenphysik, Karlsruhe Institute of Technology (KIT),
76128 Karlsruhe, Germany
Institute for Nuclear Research, Russian Academy of Sciences,
119899 Moscow, Russia
E-Mail: `penin@ualberta.ca`

Jan H. Piclum

Institut für Theoretische Teilchenphysik und Kosmologie, RWTH Aachen,
52056 Aachen, Germany
E-Mail: `piclum@physik.rwth-aachen.de`

ABSTRACT: We develop a systematic approach to describe the finite lifetime effects in the threshold production of top quark-antiquark pairs. It is based on the nonrelativistic effective field theory with an additional scale $\rho^{1/2} m_t$ characterizing the dynamics of the top-quark decay, which involves a new expansion parameter $\rho = 1 - m_W/m_t$. Our method naturally resolves the problem of spurious divergences in the analysis of the unstable top production. Within this framework we compute the next-to-leading nonresonant contribution to the total cross section of the top quark-antiquark threshold production in electron-positron annihilation through high-order expansion in ρ and confirm the recently obtained result. We extend the analysis to the next-to-next-to-leading $\mathcal{O}(\alpha_s)$ nonresonant contribution which is derived in the leading order in ρ. The dominant nonresonant contribution to the top-antitop threshold production in hadronic collisions is also obtained.

arXiv:1110.1970v2 [hep-ph] 23 Jul 2012

Contents

1. Introduction

The threshold production of top quark-antiquark pairs at a future linear collider may provide us with the most accurate information on the top-quark mass and couplings crucial for our understanding of electroweak symmetry breaking and mass generation mechanism [1]. Due to renormalization group suppression of the strong coupling the nonrelativistic top-antitop pair is the cleanest quarkonium-like system. Its theoretical description is entirely based on the first principles of QCD and is an ideal laboratory to develop the nonrelativistic effective field theory approach. It is not surprising that since the pioneering papers [2, 3, 4] the top-antitop threshold production remains in the focus of theoretical research for over two decades. A significant progress has been achieved in the analysis of the higher order perturbative and relativistic corrections in the strong coupling constant α_s and the heavy-quark velocity v. Sizable next-to-next-to-leading order (NNLO) corrections to the total cross section have been found by several groups [5, 6, 7, 8, 9] that stimulated the study of the higher orders of perturbation theory. Currently a bulk of the third order corrections is available [11, 10, 12, 13, 14, 15, 16, 17, 18, 19, 20, 21, 22, 23, 24] with only a few Wilson coefficients still missing, and the N^{3}LO analysis is likely to be completed in the foreseeable future. Moreover the higher order logarithmically enhanced corrections have been resummed through the effective theory renormalization group methods [25, 26, 27].

At the same time much less attention has been paid to the analysis of the effects related to the instability of the top quark [28, 29, 30, 31]. The width of the electroweak top-quark decay $t \to W^+ b$, $\Gamma_t \approx 1.5$ GeV, is comparable to the binding energy of a would-be toponium

ground state and has a dramatic effect on the threshold production. It serves as an infrared cutoff, which makes the process perturbative in the whole threshold region, and smears out all the Coulomb-like resonances below the threshold leaving a single well pronounced peak in the cross section. The standard prescription in the analysis of the unstable top-quark production consists of the complex shift $E \to E + i\Gamma_t$, where E is the top-antitop pair energy counted from the threshold [2]. Though this procedure incorporates the dominant effect of the finite top-quark width, it does not fully account for nonresonant processes like $e^+e^- \to tW^-\bar{b}$, $e^+e^- \to bW^+\bar{t}$ or $e^+e^- \to W^+W^-b\bar{b}$ where the intermediate top quark is not on its (complex) mass shell. Such processes *cannot be distinguished* from the resonant $t\bar{t}$ production, which has the same final states due to the top-quark instability. Moreover, a naïve use of the above prescription results in spurious divergences of the cross section in the nonrelativistic effective field theory [28, 30] and it has to be elaborated to make the high-order calculations self-consistent. Recently two different approaches have been used to refine the analysis of the finite width effect. The first is based on so-called "phase space matching" [32] while the second [33] relies on the effective theory of unstable particles [34]. In particular, in ref. [33] the NLO nonresonant contribution to the total cross section has been computed.

In the present paper we develop an alternative approach which systematically takes into account the effect of top-quark instability. The approach is applicable to the threshold production of an unstable particle which is almost degenerate in mass with one of its decay products. It introduces into the nonrelativistic effective field theory [35, 36] an additional scale $\rho^{1/2}m_t$ characterizing the dynamics of the top-quark decay into a nonrelativistic W-boson and an ultrarelativistic bottom quark. The parameter ρ is related to the difference of the top quark and W-boson masses, $\rho = 1 - m_W/m_t$, and $\rho^{1/2}$ plays the role of the heavy quark velocity in standard potential nonrelativistic QCD (pNRQCD) [37, 38]. The new scale obeys the hierarchy $vm_t \ll \rho^{1/2}m_t \ll m_t$ or $v \ll \rho^{1/2} \ll 1$ and the cross section is constructed as a series in the scale ratios. The method is applicable for the analysis of the high order corrections and naturally resolves the problem of the spurious divergences.

In the next section we outline the main concept and derive the NLO nonresonant contribution to the total cross section in the leading order in ρ. In section 3 we describe the calculation of the high order terms of the expansion. The strong coupling corrections to the result of section 2 are computed in section 4. In section 5 we show how the spurious effective theory divergences associated with the top-quark instability are eliminated within our approach. Section 6 collects the final result and numerical estimates. Application of our result to the analysis of the experimentally measured cross section with invariant mass cuts is discussed in section 7. Section 8 is our conclusion.

2. Finite width effect beyond the complex energy shift

In the Born approximation the total cross section of top-antitop production in electron-positron annihilation is related through the optical theorem to the imaginary part of the one-loop forward scattering amplitude shown in figure 1. The corresponding expression for the normalized cross section $R = \sigma(e^+e^- \to t\bar{t})/\sigma_0$, $\sigma_0 = 4\pi\alpha^2/(3s)$, in the threshold
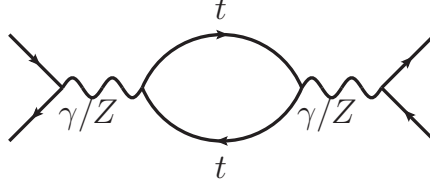
Figure 1: e^+e^- forward scattering diagram corresponding to the leading order top-quark pair production process.

region $s \approx 4m_t^2$ can be obtained by the standard nonrelativistic expansion of the top-quark vertices and propagators in v and reads

$$R_{res}^{Born} = \left[Q_e^2 Q_t^2 + \frac{2Q_e Q_t v_e v_t}{1 - x_Z} + \frac{(a_e^2 + v_e^2)v_t^2}{(1 - x_Z)^2} \right] \frac{6\pi N_c}{m_t^2} \mathrm{Im}[G_0(0, 0, E + i\varepsilon)] + \dots , \quad (2.1)$$

where the ellipsis stands for the relativistic corrections, Q_f is the electric charge of fermion f in units of the positron charge, $N_c = 3$ is the number of colors, and $x_Z = m_Z^2/(4m_t^2)$ with the Z-boson mass m_Z. The couplings of fermion f to the Z-boson are

$$v_f = \frac{I_{w,f}^3 - 2s_w^2 Q_f}{2s_w c_w} , \qquad a_f = \frac{I_{w,f}^3}{2s_w c_w} , \qquad (2.2)$$

where $I_{w,f}^3$ is the third component of the fermion's weak isospin and s_w (c_w) is the sine (cosine) of the weak mixing angle. Note that only the vector coupling of the top quark gives the leading order contribution and the axial coupling is suppressed by an additional power of v. The last factor in eq. (2.1) is

$$G_0(0, 0, E) = \int \frac{\mathrm{d}^{d-1}\boldsymbol{p}}{(2\pi)^{d-1}} \frac{m_t}{\boldsymbol{p}^2 - m_t E} = -\frac{m_t^2}{4\pi} \sqrt{\frac{-E}{m_t}} , \qquad (2.3)$$

which is nothing but the Green's function of the free Schrödinger equation at the origin. Formally the integral in eq. (2.3) is linearly divergent but the divergent part is real and does not contribute to the cross section. To handle the divergence we use dimensional regularization with $d = 4 - 2\epsilon$, where the integral (2.3) is finite even for $\epsilon = 0$. The strong interaction has a significant impact on the threshold cross section. Close to threshold when $v \sim \alpha_s$ the Coulomb effects become nonperturbative and have to be resummed to all orders in α_s by substituting eq. (2.3) with the full Coulomb Green's function

$$G_C(0, 0; E) = G_0(0, 0; E) + G_1(0, 0; E) - \frac{C_F \alpha_s m_t^2}{4\pi} \left[\Psi \left(1 - \frac{C_F \alpha_s}{2} \sqrt{\frac{m_t}{-E}} \right) + \gamma_E \right] , \qquad (2.4)$$

where Ψ is the logarithmic derivative of the Gamma function and $C_F = 4/3$. The one-gluon exchange contribution $G_1(0, 0; E)$ is ultraviolet divergent. Again for stable top quarks the divergent part is real and does not contribute to eq. (2.1). In the $\overline{\mathrm{MS}}$ subtraction scheme this term reads

$$G_1(0, 0; E) = -\frac{C_F \alpha_s m_t^2}{8\pi} \left[\ln \left(\frac{-m_t E}{\mu^2} \right) - 1 + 2\ln 2 \right] . \qquad (2.5)$$

Let us now consider the top-quark decay. Every decay process is suppressed by the electroweak coupling constant α_{ew}. We adopt the standard power counting rules $\alpha_s \sim v$, $\alpha_{ew} \sim v^2$. Thus to NNLO if the top quark decays the antiquark may be treated as a stable particle and vice versa. The dominant effect of the top-quark instability is related to the imaginary part of its mass operator in diagram $2(a)$. In the massless bottom quark approximation and with the off-shell momentum p the mass operator reads

$$\text{Im}[\Sigma^{(0)}(p^2)] = \frac{G_F}{16\pi\sqrt{2}} p^3 \left(1 + 2\frac{m_W^2}{p^2}\right)\left(1 - \frac{m_W^2}{p^2}\right)^2 \theta(p^2 - m_W^2), \tag{2.6}$$

where G_F is the Fermi constant and we use the approximation $V_{tb} = 1$. Close to the mass shell one has $p^2 = m_t^2 - 2(\boldsymbol{p}^2 - m_t E) + \ldots$, where $\boldsymbol{p}$ is the spatial momentum of the top quark, and the mass operator can be expanded in $z = (\boldsymbol{p}^2 - m_t E)/m_t^2 \ll 1$

$$\begin{aligned}
\text{Im}[\Sigma^{(0)}(z)] &= \frac{\Gamma_t}{2}\left(1 - \frac{4z}{(1-x^2)} + \frac{4z^2}{(1-x^2)^2}\right)\theta(1 - x^2 - 2z) + \ldots \\
&= \frac{\Gamma_t}{2} - \frac{\Gamma_t}{2}\left[\theta(x^2 + 2z - 1) + \left(\frac{4z}{(1-x^2)} - \frac{4z^2}{(1-x^2)^2}\right)\theta(1 - x^2 - 2z)\right] + \ldots.
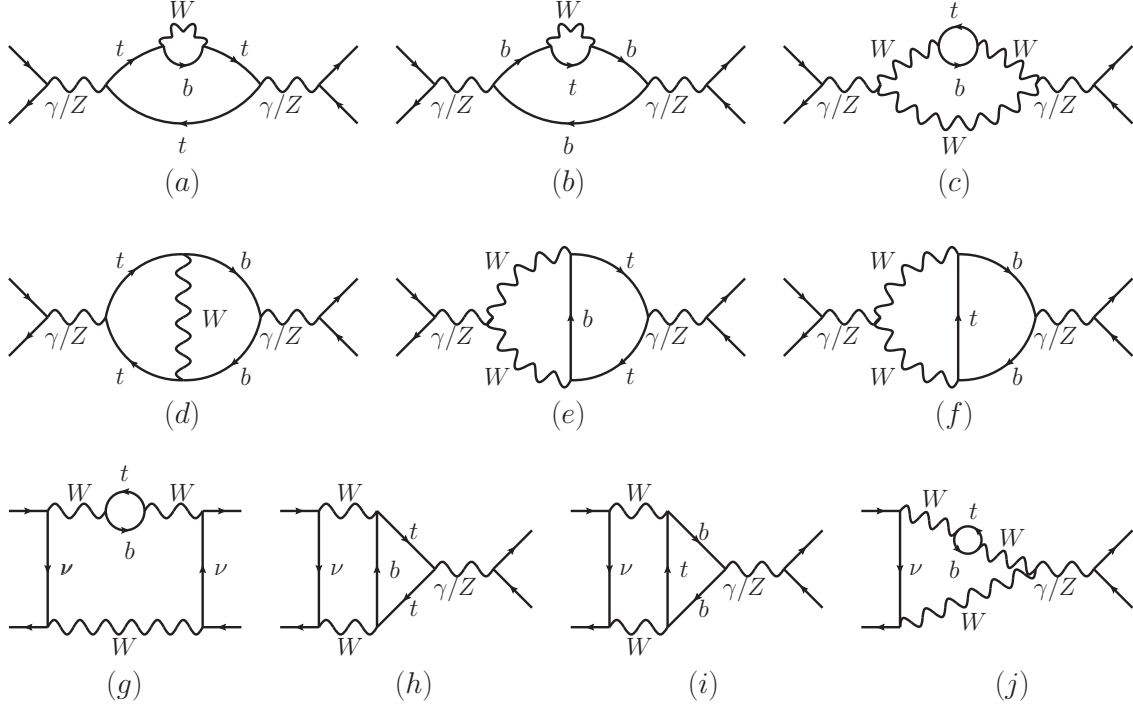\end{aligned} \tag{2.7}$$

where $x = m_W/m_t$, $\Gamma_t = \Gamma_t^{(0)} + \mathcal{O}(\alpha_s)$ and

$$\Gamma_t^{(0)} = \frac{G_F m_t^3}{8\pi\sqrt{2}}(1 + 2x^2)(1 - x^2)^2, \tag{2.8}$$

is the leading order top-quark electroweak width. Note that in the expansion (2.7) we consider $1 - x = \rho$ to be of the same order of magnitude as z. The first term in the last line of eq. (2.7) describes the standard shift of the pole position of the top quark propagator into the unphysical sheet of the complex energy plane characteristic for unstable particles. After Dyson resummation it replaces the argument of eq. (2.3) by $E + i\Gamma_t$, which is the original prescription of ref. [2]. Eq. (2.7), however, has the remainder which also contributes to the imaginary part of the forward scattering amplitude. Since the remainder vanishes for on-shell top quark, it represents the nonresonant process $e^+e^- \to bW^+\bar{t}$ or $e^+e^- \to tW^-\bar{b}$.

In the nonresonant contribution the integral over the virtual momentum $\boldsymbol{p}$ is saturated by the region $|\boldsymbol{p}| \sim \rho^{1/2}m_t$. The main idea of our approach is that if ρ is considered as a small parameter this momentum region corresponds to a nonrelativistic top quark with the energy $p_0 - m_t \sim \boldsymbol{p}^2/m_t \sim \rho m_t$, and one may apply the well elaborated pNRQCD tools for the calculation of the cross section. In this complementary nonrelativistic expansion the heavy quark velocity v is replaced by $\rho^{1/2}$ and we have the hard scale m_t, the soft scale $\rho^{1/2}m_t$, and the ultrasoft scale ρm_t. Note that in this case the W-boson is also nonrelativistic while the bottom quark is ultrarelativistic with the ultrasoft four-momentum of order $\rho m_t \gg m_b$. Further expansion of eq. (2.7) in $\rho \sim z$ gives

$$\text{Im}[\Sigma^{(0)}(z)] = \frac{\Gamma_t}{2} - \frac{\Gamma_t}{2}\left[\theta(z - \rho) + \left(\frac{2z}{\rho} - \frac{z^2}{\rho^2}\right)\theta(\rho - z) + \mathcal{O}(\rho, z)\right]. \tag{2.9}$$

Figure 2: e^+e^- forward scattering diagrams containing $bW^+\bar{t}$ and $tW^-\bar{b}$ cuts.

By inserting the second term of eq. (2.9) into the diagram 2(a) one obtains the following contribution to the nonresonant cross section

$$R_1 = \left[Q_e^2 Q_t^2 + \frac{2Q_e Q_t v_e v_t}{1 - x_Z} + \frac{(a_e^2 + v_e^2) v_t^2}{(1 - x_Z)^2} \right] \frac{N_c \Gamma_t}{m_t} \delta_1 (1 + \mathcal{O}(\rho)), \qquad (2.10)$$

where $\delta_1 = \delta_1^{(0)} + \mathcal{O}(\alpha_s)$. The leading order result reads

$$\delta_1^{(0)} = -6\pi \left[\int \frac{\mathrm{d}^3 \boldsymbol{p}}{(2\pi)^3} \theta(\boldsymbol{p}^2 - \rho m_t^2) \frac{m_t}{\boldsymbol{p}^4} + \int \frac{\mathrm{d}^3 \boldsymbol{p}}{(2\pi)^3} \theta(\rho m_t^2 - \boldsymbol{p}^2) \left(\frac{2}{\rho} \frac{\boldsymbol{p}^2}{m_t^2} - \frac{1}{\rho^2} \frac{\boldsymbol{p}^4}{m_t^4} \right) \frac{m_t}{\boldsymbol{p}^4} \right]$$

$$= -\frac{8}{\pi} \frac{1}{\rho^{1/2}} . \qquad (2.11)$$

In eq. (2.11) we neglect the $m_t E$ term in z since it gives a subleading contribution suppressed by $m_t E/\boldsymbol{p}^2 \sim v^2/\rho \ll 1$ according to our scale hierarchy. Note that one can obtain the result (2.11) without subtracting the first term of eq. (2.9) by direct evaluation of the corresponding Feynman integral in dimensional regularization. In this case the resonance contribution vanishes since eq. (2.3) becomes a scaleless integral.

Eq. (2.10) however does not give the full nonresonant contribution and one has to take into account all diagrams of this order with the $bW^+\bar{t}$ or $tW^-\bar{b}$ cuts given in figure 2. The calculation is significantly simplified within the nonrelativistic effective theory where all the propagators which are off-shell by the amount m_t collapse, giving rise to new effective theory vertices. From the practical point of view, however, it is more convenient to directly expand

the full theory Feynman integrals in ρ than to use the effective theory Feynman rules. We found that beside diagram $2(a)$ only diagram $2(g)$ gives a leading order contribution in ρ. After the expansion the off-shell neutrino propagators shrink to points and the diagram becomes similar to figure $2(a)$. In this case the contribution comes from the imaginary part of the vacuum polarization operator of the heavy-light vector current correlator

$$\text{Im}[\Pi^{(0)}(p^2)] = \frac{N_c}{24\pi} \left(2 + \frac{m_t^2}{p^2}\right) \left(1 - \frac{m_t^2}{p^2}\right)^2 \theta(p^2 - m_t^2), \tag{2.12}$$

where $p^2 = 2m_t^2 - m_W^2 - 2(\boldsymbol{p}^2 - m_t E) + \dots$. It has the following expansion

$$\text{Im}[\Pi^{(0)}(z)] = \frac{N_c \rho^2}{2\pi} \left[\left(1 - \frac{z}{\rho}\right)^2 \theta(\rho - z) + \mathcal{O}(\rho, z)\right]. \tag{2.13}$$

The corresponding contribution to the nonresonant cross section reads

$$R_2 = \frac{1}{s_w^4} \frac{N_c \Gamma_t}{m_t} \delta_2 (1 + \mathcal{O}(\rho)), \tag{2.14}$$

where

$$
\begin{aligned}
\delta_2^{(0)} &= 2\pi \int \frac{\mathrm{d}^3\boldsymbol{p}}{(2\pi)^3} \theta(\rho m_t^2 - \boldsymbol{p}^2) \left(1 - \frac{\boldsymbol{p}^2}{\rho m_t^2}\right)^2 \frac{m_t}{(2\rho m_t^2 - \boldsymbol{p}^2)^2} \\
&= \left(\frac{17}{6} - \frac{9\sqrt{2}}{4} \ln\left(1 + \sqrt{2}\right)\right) \frac{1}{\pi} \frac{1}{\rho^{1/2}}.
\end{aligned}
\tag{2.15}
$$

Each W-boson propagator brings a factor $(2\rho m_t^2 - \boldsymbol{p}^2)^{-1}$ to eq. (2.15) which is regular at $\boldsymbol{p}^2 = 0$ so that the diagram does not have a resonance contribution. Finally for the leading nonresonant contribution to the cross section we get

$$
\begin{aligned}
R_{nr} = -\frac{8N_c}{\pi \rho^{1/2}} \frac{\Gamma_t}{m_t} &\left[\left(Q_e^2 Q_t^2 + \frac{2Q_e Q_t v_e v_t}{1 - x_Z} + \frac{(a_e^2 + v_e^2)v_t^2}{(1 - x_Z)^2}\right)\right. \\
&\left. - \frac{1}{s_w^4}\left(\frac{17}{48} - \frac{9\sqrt{2}}{32} \ln\left(1 + \sqrt{2}\right)\right) + \mathcal{O}(\rho, \alpha_s)\right].
\end{aligned}
\tag{2.16}
$$

Let us now compare our approach to the one of [33]. In ref. [33] the scales m_t and $\rho^{1/2} m_t$ are considered to be of the same order and are integrated out simultaneously. As a result the nonresonant contribution is represented by the imaginary part of the Wilson coefficient of the local four-fermion $e^+e^-e^+e^-$ operators, i.e. every diagram in figure 2 shrinks to a point. The method requires more complex calculations but gives the exact dependence of the cross section on ρ. However, in the next section we show how to compute a sufficient number of terms of the expansion in ρ to ensure very good accuracy of the approximation for the physical value $\rho \approx 0.53$. At the same time application of the method [33] to the calculation of the strong interaction corrections to the nonresonant contribution seems to become technically complicated while our approach does not as we show in section 4.

3. Relativistic corrections

To obtain the high order terms of the nonrelativistic expansion of the nonresonant cross section in ρ we use the method of regions [39, 40]. By the optical theorem the problem is reduced to the calculation of the contribution from $bW^+\bar{t}$ and $tW^-\bar{b}$ cuts to the imaginary part of the two-loop electron-positron forward scattering amplitude, figure 2. As an example let us describe the evaluation of diagram $2(e)$. The corresponding scalar integral reads

$$\int \frac{\mathrm{d}^d k \, \mathrm{d}^d l}{(l^2 + i\varepsilon)(k^2 + q \cdot k + i\varepsilon)(k^2 - q \cdot k + i\varepsilon)[(k + l)^2 + q \cdot (k + l) + m_t^2 \rho(2 - \rho) + i\varepsilon]}$$
$$\times \frac{1}{[(k + l)^2 - q \cdot (k + l) + m_t^2 \rho(2 - \rho) + i\varepsilon]}, \tag{3.1}$$

where $q = (2m_t, \mathbf{0})$ is the photon/Z-boson momentum corresponding to the top-antitop threshold. In the limit $\rho \to 0$ the only nonvanishing contribution to the imaginary part comes from the region of potential momentum k and ultrasoft momentum l

$$k_0 \sim m_t \rho, \qquad \mathbf{k} \sim m_t \rho^{1/2}, \qquad l \sim m_t \rho. \tag{3.2}$$

By imposing this scaling we expand eq. (3.1) in ρ. For example in the leading order we obtain

$$\int \frac{\mathrm{d}k_0 \, \mathrm{d}^{d-1}\mathbf{k} \, \mathrm{d}l_0 \, \mathrm{d}^{d-1}\mathbf{l}}{(l^2 + i\varepsilon)(-\mathbf{k}^2 + 2m_t k_0 + i\varepsilon)(-\mathbf{k}^2 - 2m_t k_0 + i\varepsilon)[-\mathbf{k}^2 + 2m_t(k_0 + l_0) + 2m_t^2 \rho + i\varepsilon]}$$
$$\times \frac{1}{[-\mathbf{k}^2 - 2m_t(k_0 + l_0) + 2m_t^2 \rho + i\varepsilon]}. \tag{3.3}$$

Then we evaluate the integrals over the zero components of the loop momenta by closing the integration contours in the upper half of the corresponding complex planes. At this step we have to distinguish between the different cuts of the diagram and pick up only those poles which correspond to $bW^+\bar{t}$ and $tW^-\bar{b}$ cuts. The integral over $\mathbf{k}$ becomes a one-loop massive tadpole integral in $d - 1$ dimensions and can be performed easily. Integration over $\mathbf{l}$ yields a Gauss hypergeometric function $_2\mathrm{F}_1$ with half-integer parameters, which can be expanded in ϵ with the `Mathematica` package `HypExp 2` [41].

The apparently more complicated diagrams $2(g)$–$2(j)$ with t-channel neutrino propagators do not pose any new problems since the off-shell neutrino propagators do not depend on the loop momentum after the expansion and the resulting integrals can be computed in the same way. We use `QGRAF` [42], `q2e`, and `exp` [43, 44] to generate the diagrams and produce `FORM`-readable expressions for the amplitudes. The expansions and integrations are performed with custom code written in `FORM` [45]. The result of the calculation is presented in section 6.

4. Strong coupling corrections

In the leading order in ρ the α_s corrections are obtained by the gluon dressing of diagrams $2(a)$ and $2(g)$ shown in figure 3. Since the top quark is nonrelativistic we can apply
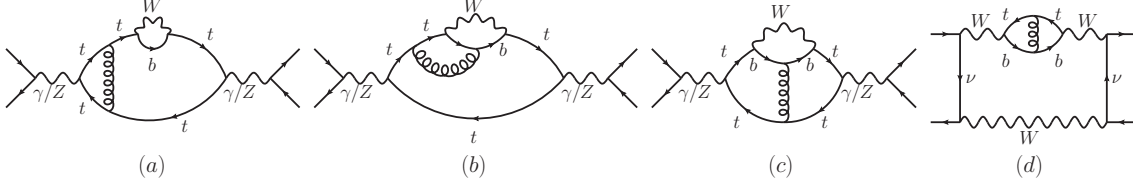
Figure 3: e^+e^- forward scattering diagrams contributing to the $\mathcal{O}(\alpha_s)$ correction in the leading order in ρ. The curly lines denote gluons.

the standard pNRQCD arguments to identify the relevant regions of virtual momentum. For diagram 3(a) the leading contribution comes from the Coulomb gluon with the potential momentum $q_0 \sim \boldsymbol{q}^2/m_t \sim \rho m_t$. As in the case of the Coulomb gluon exchange in pNRQCD, the corresponding correction is power enhanced due to the Coulomb singularity but the enhancement factor here is $1/\rho^{1/2}$ rather than $1/v$. An important difference with respect to pNRQCD is that since $\alpha_s/\rho^{1/2} \ll 1$ one does not need to resum the Coulomb corrections to all orders. Following the analysis of section 2 one gets the potential Coulomb gluon contribution of the following form

$$
\left.\delta_{1a}^{(1)}\right|_{\rho^{-1}} = -12\pi\mathrm{Re}\left\{ \int \frac{\mathrm{d}^3\boldsymbol{p}}{(2\pi)^3} \frac{\mathrm{d}^3\boldsymbol{p}'}{(2\pi)^3} \frac{m_t}{(\boldsymbol{p}^2 - m_t(E+i\Gamma_t))^2} \frac{m_t}{\boldsymbol{p}'^2 - m_t(E+i\Gamma_t)} \frac{4\pi C_F \alpha_s}{(\boldsymbol{p}-\boldsymbol{p}')^2} \right.
$$

$$
\left. \times \left[\theta(\boldsymbol{p}^2 - \rho m_t^2) + \theta(\rho m_t^2 - \boldsymbol{p}^2)\left(\frac{2}{\rho}\frac{\boldsymbol{p}^2}{m_t^2} - \frac{1}{\rho^2}\frac{\boldsymbol{p}^4}{m_t^4} \right) \right] \right\}
$$

$$
= 3\left(L_E + \frac{1}{2} + 2\ln 2 \right)\frac{C_F \alpha_s}{\rho}\,, \tag{4.1}
$$

where $L_E = \ln\left(\frac{\sqrt{E^2+\Gamma_t^2}}{\rho m_t} \right)$ and $\delta_1^{(1)}$ defines the correction to eq. (2.10), $\delta_1 = \delta_1^{(0)} + \delta_1^{(1)} + \mathcal{O}(\alpha_s^2)$. Note that one has to keep a nonzero (complex) energy in the top-quark propagator in eq. (4.1) since it serves as an infrared regulator. The contribution of the hard gluon with momentum $q \sim m_t$ in diagram 3(a) can be related to the Wilson coefficient in the nonrelativistic expansion of the vector current j_μ

$$
\boldsymbol{j} = c_v\psi^\dagger\boldsymbol{\sigma}\chi + \frac{d_v}{6m^2}\psi^\dagger\boldsymbol{\sigma}\boldsymbol{D}^2\chi + \dots\,, \tag{4.2}
$$

where ψ and χ are the nonrelativistic quark and antiquark two-component Pauli spinors and the Wilson (matching) coefficients are $c_v = 1 - 2C_F\alpha_s/\pi + \dots$ and $d_v = 1 + \dots$. The $\mathcal{O}(\alpha_s)$ term in c_v results in the following correction to δ_1 in eq. (2.3)

$$
\left.\delta_{1a}^{(1)}\right|_{\rho^{-1/2}} = -\frac{4C_F\alpha_s}{\pi}\delta_1^{(0)} = 32\frac{C_F\alpha_s}{\pi^2}\frac{1}{\rho^{1/2}}\,. \tag{4.3}
$$

Diagram 3(b) is determined by the correction to the mass operator in the limit $z \to 0$ that can be read off the result of ref. [46]

$$
\mathrm{Im}[\Sigma^{(1)}(z)] = \frac{C_F\alpha_s}{\pi}\left[\frac{9}{4} - \frac{2}{3}\pi^2 - \frac{3}{2}\ln(2\rho) - \frac{3}{2}\ln\left(1 - \frac{z}{\rho}\right) + \mathcal{O}(\rho, z) \right]\mathrm{Im}[\Sigma^{(0)}(z)]\,. \tag{4.4}
$$

The correction factor should in principle be substituted into the integral (2.11). However all the terms in eq. (4.4) except the last logarithmic one actually describe the corrections to the top-quark width [46], $\Gamma_t = \Gamma_t^{(0)} + \Gamma_t^{(1)}$, where

$$\Gamma_t^{(1)} = \frac{C_F \alpha_s}{\pi} \left(\frac{9}{4} - \frac{2}{3}\pi^2 - \frac{3}{2}\ln(2\rho) + \mathcal{O}(\rho) \right) \Gamma_t^{(0)} . \tag{4.5}$$

They all disappear when the leading order top-quark width in eq. (2.10) is replaced with its corrected (physical) value. The remaining term gives

$$\begin{aligned}
\delta_{1b}^{(1)} &= -9C_F\alpha_s \int \frac{\mathrm{d}^3\boldsymbol{p}}{(2\pi)^3} \theta(\rho m_t^2 - \boldsymbol{p}^2) \left(1 - \frac{\boldsymbol{p}^2}{\rho m_t^2} \right)^2 \ln\left(1 - \frac{\boldsymbol{p}^2}{\rho m_t^2} \right) \frac{m_t}{\boldsymbol{p}^4} \\
&= -2\,(7 - 12\ln 2)\, \frac{C_F\alpha_s}{\pi^2} \frac{1}{\rho^{1/2}} .
\end{aligned} \tag{4.6}$$

The same procedure applies to diagram 3(d) which is determined by the correction to the polarization function [47]

$$\mathrm{Im}[\Pi^{(1)}(z)] = \frac{C_F\alpha_s}{\pi} \left[\frac{9}{4} + \frac{1}{3}\pi^2 - \frac{3}{2}\ln(2\rho) - \frac{3}{2}\ln\left(1 - \frac{z}{\rho} \right) + \mathcal{O}(\rho, z) \right] \mathrm{Im}[\Pi^{(0)}(z)]. \tag{4.7}$$

After factoring out the corrections to the top-quark width one gets

$$\begin{aligned}
\delta_2^{(1)} &= C_F\alpha_s \left[\pi\delta_2^{(0)} - 3\int \frac{\mathrm{d}^3\boldsymbol{p}}{(2\pi)^3} \theta(\rho m_t^2 - \boldsymbol{p}^2) \left(1 - \frac{\boldsymbol{p}^2}{\rho m_t^2} \right)^2 \ln\left(1 - \frac{\boldsymbol{p}^2}{\rho m_t^2} \right) \frac{m_t}{(2\rho m_t^2 - \boldsymbol{p}^2)^2} \right] \\
&= \left[\frac{22}{3} + \frac{17\pi^2}{6} - \frac{17}{2}\ln 2 + \left(2 - 3\pi^2 + 9\ln 2 \right) \frac{3\sqrt{2}}{4}\ln\left(1 + \sqrt{2} \right) \right. \\
&\quad \left. - \frac{27\sqrt{2}}{8}\left(\ln^2\left(1 + \sqrt{2} \right) + \mathrm{Li}_2\left(2\sqrt{2} - 2 \right) \right) \right] \frac{C_F\alpha_s}{\pi^2} \frac{1}{\rho^{1/2}} ,
\end{aligned} \tag{4.8}$$

where Li_2 stands for the dilogarithm function.

The potential gluon contribution to the nonfactorizable diagram 3(c) in the leading order in v vanishes for the total cross section [29]. The hard gluon contribution to this diagram is power suppressed. Thus the diagram vanishes in our approximation. This completes the calculation of the dominant $\mathcal{O}(\alpha_s)$ corrections. In the next section, however, we present the analysis of the corrections suppressed by an additional power of $\rho^{1/2}$ which addresses an important issue of the spurious divergences in the nonrelativistic effective theory of unstable top-quark production.

5. Eliminating the spurious divergences

Let us first outline the problem. In the pNRQCD perturbation theory the Coulomb Green's function gets corrections due to the second term of eq. (4.2) and from the relativistic corrections to the Coulomb Hamiltonian

$$\delta\mathcal{H} = -\frac{\boldsymbol{\partial}^4}{4m_q^3} + \frac{C_F\alpha_s}{2m_q^2}\left\{ \boldsymbol{\partial}^2, \frac{1}{x} \right\} , \tag{5.1}$$

of the following form

$$\delta G_1(0,0;E) = \frac{5}{3}\frac{E}{m_t}G_1(0,0;E)\,. \tag{5.2}$$

As it has been pointed out the Green's function in the above equation is divergent and in dimensional regularization reads

$$
\begin{aligned}
G_1^\epsilon(0,0;E) &= \int \frac{\mathrm{d}^{d-1}\boldsymbol{p}}{(2\pi)^{d-1}}\frac{\mathrm{d}^{d-1}\boldsymbol{p}'}{(2\pi)^{d-1}}\frac{m_t}{\boldsymbol{p}^2 - m_t E}\frac{m_t}{\boldsymbol{p}'^2 - m_t E}\frac{4\pi C_F\alpha_s}{(\boldsymbol{p}-\boldsymbol{p}')^2}\\
&= -\frac{C_F\alpha_s m_t^2}{8\pi}\left[-\frac{1}{2\epsilon}+\ln\left(\frac{-m_t E}{\mu^2}\right)-1+2\ln 2+\mathcal{O}(\epsilon)\right],
\end{aligned}\tag{5.3}
$$

where the standard $\overline{\mathrm{MS}}$ factor $\left(\frac{\mu^2 e^{\gamma_E}}{4\pi}\right)^\epsilon$ per loop is suppressed. For real energy values the divergent part of eq. (5.2) is real and does not contribute to the cross section. After the complex energy shift the divergence gets the imaginary part proportional to Γ_t

$$
\begin{aligned}
\mathrm{Im}[\delta G_1^\epsilon(0,0;E+i\Gamma_t)]_{\Gamma_t} &= \frac{5}{3}\frac{\Gamma_t}{m_t}\,\mathrm{Re}[G_1^\epsilon(0,0;E+i\Gamma_t)]\\
&= -\frac{5}{24}\left[-\frac{1}{2\epsilon}+\ln\left(\frac{m_t\sqrt{E^2+\Gamma_t^2}}{\mu^2}\right)-1+2\ln 2+\mathcal{O}(\epsilon)\right]\frac{C_F\alpha_s}{\pi}m_t\Gamma_t
\end{aligned}\tag{5.4}
$$

resulting in a divergent cross section. In the previous analysis the Green's function was renormalized, as in eq. (2.5), leaving a finite but scheme-dependent cross section. The solution of this problem is straightforward within our approach. Indeed the logarithmically divergent integral in eq. (5.4) has a physical cutoff scale $\rho^{1/2}m_t$ where the imaginary part of the top-quark mass operator vanishes. In the above expression this scale is set to infinity. Thus within the expansion by regions framework eq. (5.4) represents a contribution of the pNRQCD potential momentum region $|\boldsymbol{p}|\sim\sqrt{m_t E}$. To get the total result one has to add the contribution of the additional potential region $|\boldsymbol{p}|\sim\rho^{1/2}m_t$. The latter is given by the interference of the corrections to the Green's function due to the top quark mass operator (2.9) and due to the relativistic corrections to the vector current (4.2) and the Hamiltonian (5.1) in the second order of time-independent perturbation theory. The resulting integral after expansion in $E/(\rho m_t)$ is infrared divergent and in dimensional regularization reads

$$
\begin{aligned}
&\mathrm{Im}[\delta G_1^\epsilon(0,0;E)]_{|\boldsymbol{p}|\sim\rho^{1/2}m_t}\\
&= \frac{5}{3}\frac{\Gamma_t}{m_t}\int\frac{\mathrm{d}^{d-1}\boldsymbol{p}}{(2\pi)^{d-1}}\frac{\mathrm{d}^{d-1}\boldsymbol{p}'}{(2\pi)^{d-1}}\frac{m_t^2}{\boldsymbol{p}^2\boldsymbol{p}'^2}\frac{4\pi C_F\alpha_s}{(\boldsymbol{p}-\boldsymbol{p}')^2}\theta(\rho m_t^2-\boldsymbol{p}^2)\left(1-\frac{\boldsymbol{p}^2}{\rho m_t^2}\right)^2\\
&= -\frac{5}{24}\left[\frac{1}{2\epsilon}-\ln\left(\frac{\rho m_t^2}{\mu^2}\right)+\frac{5}{2}+\mathcal{O}(\epsilon)\right]\frac{C_F\alpha_s}{\pi}m_t\Gamma_t\,.
\end{aligned}\tag{5.5}
$$

In the sum of eqs. (5.4) and (5.5) the poles in ϵ cancel each other and one gets the finite result for the correction

$$\mathrm{Im}[\delta G_1(0,0;E+i\Gamma_t)]_{\Gamma_t} = -\frac{5}{24}\left[L_E+\frac{3}{2}+2\ln 2\right]\frac{C_F\alpha_s}{\pi}m_t\Gamma_t\,. \tag{5.6}$$

One formally reproduces the sum of the two regions, eq. (5.6), if in eq. (5.2) the $\overline{\text{MS}}$ renormalized Green's function (2.5) is evaluated with $\mu = e^{-5/4}\rho^{1/2}m_t$, which can be taken as a practical prescription for the calculation of the cross section. A similar analysis in the case of P-wave heavy-quarkonium production has been performed in refs. [28, 30]. Note that eq. (5.6) gives only a part of the $\mathcal{O}(\rho^{1/2}\alpha_s)$ corrections to the nonresonant cross section which corresponds to specific terms in the nonrelativistic expansion of diagram 3(a) and does not account for the axial coupling of the top quark and the higher order terms in the expansion of the mass operator as well as the contribution of other diagrams which vanish in the lower orders. The complete result for the $\mathcal{O}(\rho^{1/2}\alpha_s)$ corrections can in principle be obtained within the approach described in section 3. However, as we will see in the next section, the leading term of the expansion in ρ gives a good approximation of the total series and is sufficient for the practical applications.

6. Results

The NLO nonresonant contribution to the threshold top-antitop production in electron-positron annihilation reads

$$R_{nr}^{(0)} = -\frac{8N_c}{\pi\rho^{1/2}}\frac{\Gamma_t}{m_t}$$

$$\times \left\{ \left[Q_e^2 Q_t^2 + \frac{2Q_e Q_t v_e v_t}{1-x_Z} + \frac{(a_e^2+v_e^2)v_t^2}{(1-x_Z)^2} \right] f_a^{VV} - \left[\frac{2Q_e Q_t v_e a_t}{1-x_Z} + \frac{2(a_e^2+v_e^2)a_t v_t}{(1-x_Z)^2} \right] f_a^{VA} \right.$$

$$+ \frac{(a_e^2+v_e^2)a_t^2}{(1-x_Z)^2} f_a^{AA} + \left[Q_e^2 Q_b^2 + \frac{2Q_e Q_b v_e(a_b+v_b)}{1-x_Z} + \frac{(a_e^2+v_e^2)(a_b+v_b)^2}{(1-x_Z)^2} \right] f_b$$

$$+ \left[Q_e^2 + \frac{2Q_e v_e c_w}{s_w(1-x_Z)} + \frac{(a_e^2+v_e^2)c_w^2}{s_w^2(1-x_Z)^2} \right] f_c + \left[\frac{Q_e Q_b v_e a_t}{1-x_Z} + \frac{(a_e^2+v_e^2)a_t(a_b+v_b)}{(1-x_Z)^2} \right] f_d^A$$

$$+ \left[Q_e^2 Q_t Q_b + Q_e v_e \frac{Q_t(a_b+v_b)+Q_b v_t}{1-x_Z} + \frac{(a_b+v_b)(a_e^2+v_e^2)v_t}{(1-x_Z)^2} \right] f_d^V$$

$$+ \left[Q_e^2 Q_t + Q_e v_e \frac{Q_t c_w + v_t s_w}{s_w(1-x_Z)} + \frac{(a_e^2+v_e^2)v_t c_w}{s_w(1-x_Z)^2} \right] f_e^V - \left[\frac{Q_e v_e a_t}{1-x_Z} + \frac{(a_e^2+v_e^2)a_t c_w}{s_w(1-x_Z)^2} \right] f_e^A$$

$$+ \left[Q_e^2 Q_b + Q_e v_e \frac{Q_b c_w + (a_b+v_b)s_w}{s_w(1-x_Z)} + \frac{(a_e^2+v_e^2)(a_b+v_b)c_w}{s_w(1-x_Z)^2} \right] f_f$$

$$+ \frac{1}{s_w^4} f_g + \left[\frac{Q_e Q_t}{s_w^2} + \frac{(a_e+v_e)v_t}{s_w^2(1-x_Z)} \right] f_h^V + \frac{(a_e+v_e)a_t}{s_w^2(1-x_Z)} f_h^A$$

$$+ \left. \left[\frac{Q_e Q_b}{s_w^2} + \frac{(a_e+v_e)(a_b+v_b)}{s_w^2(1-x_Z)} \right] f_i + \left[\frac{Q_e}{s_w^2} + \frac{(a_e+v_e)c_w}{s_w^3(1-x_Z)} \right] f_j \right\}, \qquad (6.1)$$

where $f_n = f_n(\rho)$ stands for the contribution of diagram 2(n) and the superscript distinguishes the contribution of the vector and axial top-quark coupling. Each function f_n is found as a power series in ρ up to $\mathcal{O}(\rho^{12})$. A text file with the expressions for all f_n is attached to the paper's source files on the arXiv. The prefactor of eq. (6.1) is chosen in such a way that $f_a^{VV} = 1 + \mathcal{O}(\rho)$. In order to cross-check our results we also expanded the integral representations given in ref. [33] and found perfect agreement.
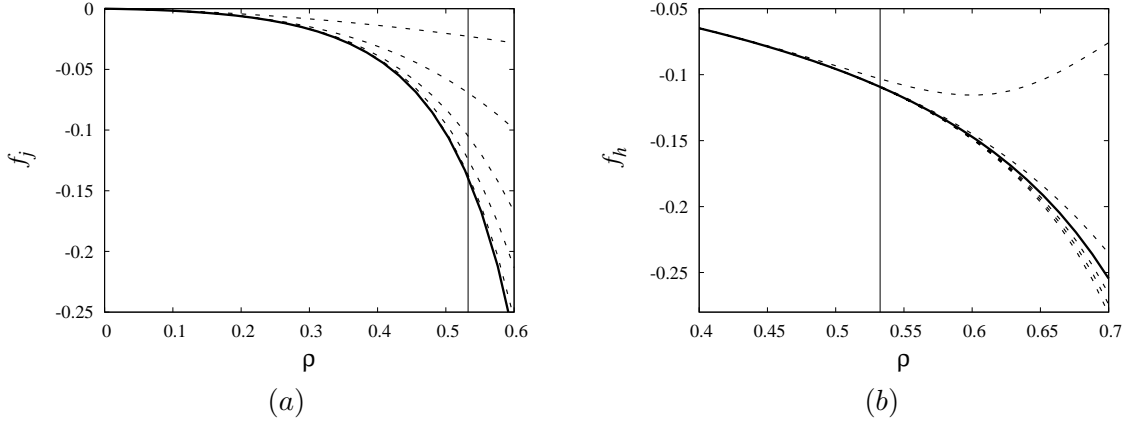
Figure 4: (a) Dashed lines represent the expansion of the function $f_j(\rho)$ in ρ through $\mathcal{O}(\rho^{2n})$ for $n = 1, \ldots, 6$. (b) Dashed lines represent the [1/11], [11/1], [9/3], [6/6], and [3/9] Padé approximants of the series for the function $f_h^V(\rho)$. In both pictures the vertical line marks the physical value of ρ and the solid curves represent the all-order numerical result of ref. [33].
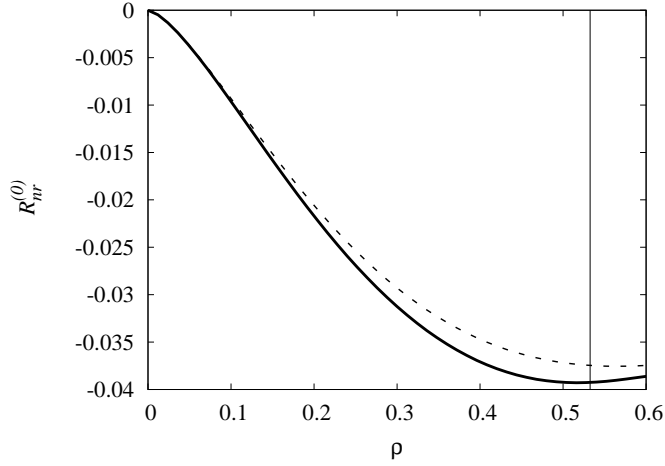
With the exception of f_h^V and f_h^A, the series converge very well for the physical value $\rho \approx 0.53$. As an example, in figure 4(a) we compare the expansion of the function f_j with the exact numerical result obtained from the integral representation given in ref. [33]. For the two special cases we perform a Padé resummation to improve the convergence, i.e. we construct the Padé approximants

$$[n/m] = \frac{\sum_{i=k}^{n} a_i \rho^i}{1 + \sum_{i=1}^{m} b_i \rho^i} , \qquad (6.2)$$

where k equals 1 and 2 for f_h^V and f_h^A, respectively. The coefficients a_i and b_i are determined by matching the expansion of eq. (6.2) in ρ to the series for f_h^V and f_h^A. In figure 4(b) we compare different Padé approximants of f_h^V with the result of ref. [33] and find perfect numerical agreement, which means that Padé resummation solves the problem of slow convergence. For our numerical analysis of the cross section we choose the approximant [9/3] for f_h^V and [8/3] for f_h^A, which deviate from the result of ref. [33] by less than one percent for the physical value of ρ.

The NNLO nonresonant contribution in the leading order in ρ is given by the $\mathcal{O}(\alpha_s)$ correction to eq. (2.16). By combining eqs. (4.1), (4.3), (4.6), and (4.8) one gets

$$
\begin{aligned}
R_{nr}^{(1)} = \frac{N_c C_F \alpha_s}{\pi^2 \rho} \frac{\Gamma_t}{m_t} \Bigg\{ & \left[Q_e^2 Q_t^2 + \frac{2 Q_e Q_t v_e v_t}{1 - x_Z} + \frac{(a_e^2 + v_e^2) v_t^2}{(1 - x_Z)^2} \right] \\
& \times \left[\left(3 L_E + \frac{3}{2} + 6 \ln 2 \right) \pi^2 + (18 + 24 \ln 2) \rho^{1/2} \right] \\
& + \frac{1}{s_w^4} \left[\frac{22}{3} + \frac{17 \pi^2}{6} - \frac{17}{2} \ln 2 + \left(2 - 3\pi^2 + 9 \ln 2 \right) \frac{3\sqrt{2}}{4} \ln \left(1 + \sqrt{2} \right) \right. \\
& \left. - \frac{27\sqrt{2}}{8} \left(\ln^2 \left(1 + \sqrt{2} \right) + \text{Li}_2 \left(2\sqrt{2} - 2 \right) \right) \right] \rho^{1/2} + \mathcal{O}(\rho) \Bigg\} .
\end{aligned}
\qquad (6.3)
$$

Figure 5: The NLO nonresonant contribution to the cross section (6.1) (solid curve) and the leading order approximation (2.16) (dashed line). The vertical line marks the physical value of ρ.

Let us now study the numerical effect of the correction. We adopt the following input values [48]

$$m_t = 172 \text{ GeV}, \qquad m_W = 80.399 \text{ GeV}, \qquad m_Z = 91.1876 \text{ GeV},$$

$$G_F = 1.16637 \cdot 10^{-5} \text{ GeV}^{-2}, \qquad \alpha_s(m_Z) = 0.1184. \tag{6.4}$$

In eq. (6.3) we use the value of the strong coupling constant $\alpha_s(\mu) = 0.1129$ corresponding to the physical normalization scale $\mu = \rho^{1/2} m_t$. This value is obtained from $\alpha_s(m_Z)$ by means of the `RunDec` program [49].

Our total result for the NLO contribution (6.1) is plotted in figure 5 as function of ρ along with the leading order term (2.16). The latter turns out to be a good approximation in the whole interval $0 < \rho < 0.6$ and deviates from the total result by less than 5% at the physical value of ρ. This justifies our approximation of the NNLO nonresonant contribution (6.3) by the leading order of the expansion in ρ. The numerical effect of the nonresonant contribution on the total threshold cross section is shown in figure 6. In this plot we use the leading order pNRQCD approximation for the resonance contribution corresponding to the Coulomb Green's function (2.4) with the strong coupling constant normalized at the soft scale $\mu_s = \alpha_s(\mu_s) C_F m_t$.

7. Measured cross section and invariant mass cuts

Experimentally the top-antitop pairs produced in electron-positron annihilation are to be reconstructed from the lepton plus four jets final state or all hadronic six jet events. Realistic simulations show that the invariant mass $p^2 = (p_W + p_b)^2$ of the three jets resulting from the bottom quark and the hadronic decay of the W-boson can be determined and the corresponding invariant mass distribution can be obtained with high accuracy [50]. The total cross section of the threshold production considered in this paper is obtained by
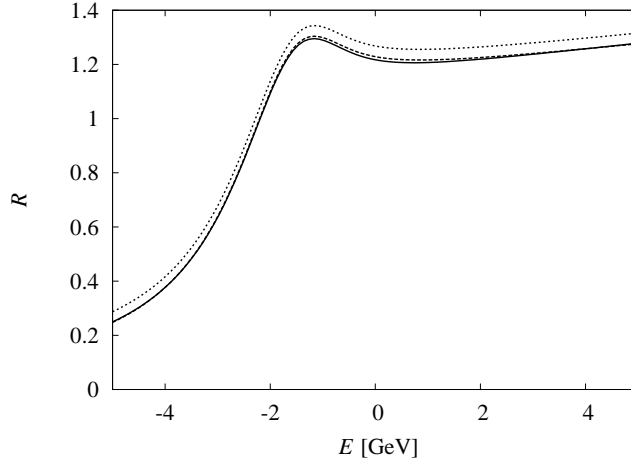
Figure 6: The normalized cross section of top-antitop production in electron-positron annihilation as function of the energy counted from the threshold. The dotted curve represents the leading order pNRQCD Coulomb approximation. The dashed curve includes the NLO nonresonant contribution and the solid curve includes the NNLO nonresonant correction as well. No strong coupling corrections to the resonance contribution are included.

integrating this distribution over the kinematically allowed interval $m_W^2 < p^2 < m_t^2$, which corresponds to the integral over $\boldsymbol{p}$ in eqs. (2.11) and (2.15). One may suggest that a tight invariant mass cut $m_t^2 - p^2 < \Lambda^2$ with $\Lambda \sim (m_t \Gamma_t)^{1/2}$ would separate the production of "true" on-shell top quark and antiquark from the nonresonant background. However, it is not possible to suppress the nonresonant contribution without significant modification of the resonant one. The resonant contribution of unstable top quark corresponds to the Breit-Wigner shape of the invariant mass distribution, which falls off rather slowly as the invariant mass deviates from m_t and is strongly affected even by loose cuts. To quantify this statement let us consider a loose cut $(m_t \Gamma_t)^{1/2} \ll \Lambda$. In the Born approximation it can be implemented by replacing the physical cutoff ρm_t^2 in the argument of the theta-functions in eqs. (2.11) and (2.15) with $\Lambda^2/2$. For $\Lambda \ll \rho^{1/2} m_t$ one gets

$$\delta_1^{(0)} = -\frac{3\sqrt{2}}{\pi} \frac{m_t}{\Lambda} + \mathcal{O}\left(\frac{\Lambda}{\rho^{1/2} m_t}\right) \tag{7.1}$$

and $\delta_2^{(0)} \sim (\Lambda/\rho^{1/2} m_t)^3$. The leading term in eq. (7.1) corresponds to the first term of eq. (2.11) and represents the modification of the resonant contribution to the cross section (2.1) by the cut. It is merely the dominant effect of the cut unless $\Lambda \sim \rho^{1/2} m_t$. The dependence of the correction to the cross section on the invariant mass cut value is shown in figure 7. Starting from $\Lambda \sim 80$ GeV it is relatively weak and the correction is well approximated by eq. (2.16). This gives a low bound on the acceptable cut value which can be used for the determination of the total cross section. One may study the cross section with tighter cuts as well. However all the high order QCD results for the total cross section are not applicable in this case and accuracy of the theoretical predictions would be significantly reduced.
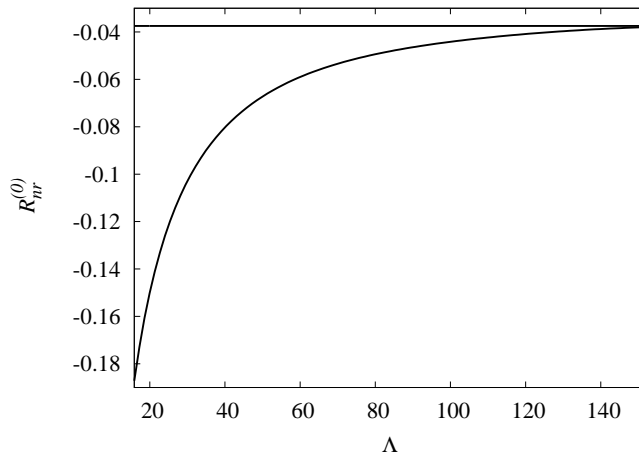
Figure 7: The nonresonant contribution as function of the cut on the three-jet final state invariant mass. The horizontal line corresponds to eq. (2.16).

8. Summary

We have developed a new method for the analysis of the top-quark instability in the threshold top quark-antiquark pair production in electron-positron annihilation based on the nonrelativistic expansion in the parameter $\rho = 1 - m_W/m_t$. Within this framework we obtain the NLO nonresonant contribution to the total threshold cross section overlooked in the standard analysis and confirm the result of ref. [33] obtained within a different effective theory approach without the expansion in ρ. The NLO contribution is negative and amounts to about 3.1% of the leading cross section above the threshold and competes with the LO contribution below the resonance region. We extend the analysis to the NNLO $\mathcal{O}(\alpha_s)$ nonresonant contribution which is computed to the leading order in ρ. The corrections involve $\ln \rho$ terms which are a new type of the large logarithms in the theory of top quark threshold production. The NNLO nonresonant contribution amounts to -0.9% at the threshold.

Our method can also be applied to the calculation of the nonresonant contribution to the threshold top quark-antiquark pair production in hadronic collisions. The process is of particular interest since a significant number of top quark-antiquark pairs is going to be produced at the LHC near the threshold and the accuracy of the top quark reconstruction is expected to be sufficiently good to study the threshold region. A comprehensive analysis of the process is given in refs. [51, 52], where the NLO approximation without the nonresonant part has been used to derive the top-antitop invariant mass distribution. The missing nonresonant contribution can be directly obtained from our result. Indeed, in the threshold region the cross section is dominated by the color singlet top-antitop configuration which is produced mainly through gluon fusion. Thus, the dominant nonresonant contribution is entirely due to the imaginary part of the top-quark mass operator and in full analogy with

eqs. (2.1) and (2.10) one gets

$$R_{nr}(\text{hadrons} \to t\bar{t}) = \frac{16}{3\pi} \left(\frac{2\Gamma_t}{\rho m_t}\right)^{\frac{1}{2}} R_{res}^{Born}(\text{hadrons} \to t\bar{t})\big|_{E=i\Gamma_t} (1 + \mathcal{O}(\rho, \alpha_s)), \quad (8.1)$$

which should be added to the resonant contribution considered in refs. [51, 52].

Acknowledgments

References

[1] M. Martinez, R. Miquel, *Multiparameter fits to the $t\bar{t}$ threshold observables at a future e^+e^- linear collider*, Eur. Phys. J. C **27** (2003) 49 [hep-ph/0207315].

[2] V. S. Fadin, V. A. Khoze, *Threshold Behavior of Heavy Top Production in e^+e^- Collisions*, JETP Lett. **46** (1987) 525.

[3] V. S. Fadin, V. A. Khoze, *Production of a pair of heavy quarks in e^+e^- annihilation in the threshold region*, Sov. J. Nucl. Phys. **48** (1988) 309.

[4] M. J. Strassler, M. E. Peskin, *The Heavy top quark threshold: QCD and the Higgs*, Phys. Rev. D **43** (1991) 1500.

[5] A. H. Hoang, T. Teubner, *Top quark pair production at threshold: Complete next-to-next-to-leading order relativistic corrections*, Phys. Rev. D **58** (1998) 114023 [hep-ph/9801397].

[6] K. Melnikov, A. Yelkhovsky, *Top quark production at threshold with $O(\alpha_s^2)$ accuracy*, Nucl. Phys. B **528** (1998) 59 [hep-ph/9802379].

[7] M. Beneke, A. Signer, V. A. Smirnov, *Top quark production near threshold and the top quark mass*, Phys. Lett. B **454** (1999) 137 [hep-ph/9903260].

[8] A. A. Penin, A. A. Pivovarov, *Analytical results for $e^+e^- \to t\bar{t}$ and $\gamma\gamma \to t\bar{t}$ observables near the threshold up to the next-to-next-to leading order of NRQCD*, Phys. Atom. Nucl. **64** (2001) 275 [hep-ph/9904278].

[9] T. Nagano, A. Ota, Y. Sumino, *$O(\alpha_s^2)$ corrections to $e^+e^- \to t\bar{t}$ total and differential cross-sections near threshold*, Phys. Rev. D **60** (1999) 114014 [hep-ph/9903498].

[10] B. A. Kniehl, A. A. Penin, *Ultrasoft effects in heavy quarkonium physics*, Nucl. Phys. B **563** (1999) 200 [hep-ph/9907489].

[11] B. A. Kniehl, A. A. Penin, *Order $\alpha_s^3 \ln^2(1/\alpha_s)$ corrections to heavy quarkonium creation and annihilation*, Nucl. Phys. B **577** (2000) 197 [hep-ph/9911414].

[12] B. A. Kniehl, A. A. Penin, V. A. Smirnov, M. Steinhauser, *Potential NRQCD and heavy quarkonium spectrum at next-to-next-to-next-to-leading order*, Nucl. Phys. B **635** (2002) 357 [hep-ph/0203166].

[13] A. A. Penin, M. Steinhauser, *Heavy quarkonium spectrum at $O(\alpha_s^5 m_q)$ and bottom / top quark mass determination*, Phys. Lett. B **538** (2002) 335 [hep-ph/0204290].

[14] B. A. Kniehl, A. A. Penin, M. Steinhauser, V. A. Smirnov, *Heavy quarkonium creation and annihilation with $\alpha_s^3 \ln(1/\alpha_s)$ accuracy*, Phys. Rev. Lett. **90** (2003) 212001 [hep-ph/0210161].

[15] A. H. Hoang, *Three loop anomalous dimension of the heavy quark pair production current in nonrelativistic QCD*, Phys. Rev. D **69** (2004) 034009 [hep-ph/0307376].

[16] A. A. Penin, V. A. Smirnov, M. Steinhauser, *Heavy quarkonium spectrum and production/annihilation rates to order $\beta_0^3 \alpha_s^3$*, Nucl. Phys. B **716** (2005) 303 [hep-ph/0501042].

[17] M. Beneke, Y. Kiyo, K. Schuller, *Third-order Coulomb corrections to the S-wave Green function, energy levels and wave functions at the origin*, Nucl. Phys. B **714** (2005) 67 [hep-ph/0501289].

[18] P. Marquard, J. H. Piclum, D. Seidel, M. Steinhauser, *Fermionic corrections to the three-loop matching coefficient of the vector current*, Nucl. Phys. B **758** (2006) 144 [hep-ph/0607168].

[19] M. Beneke, Y. Kiyo, K. Schuller, *Third-order non-Coulomb correction to the S-wave quarkonium wave functions at the origin*, Phys. Lett. B **658** (2008) 222 [arXiv:0705.4518 [hep-ph]].

[20] M. Beneke, Y. Kiyo, A. A. Penin, *Ultrasoft contribution to quarkonium production and annihilation*, Phys. Lett. B **653** (2007) 53 [arXiv:0706.2733 [hep-ph]].

[21] M. Beneke, Y. Kiyo, *Ultrasoft contribution to heavy-quark pair production near threshold*, Phys. Lett. B **668** (2008) 143 [arXiv:0804.4004 [hep-ph]].

[22] P. Marquard, J. H. Piclum, D. Seidel, M. Steinhauser, *Completely automated computation of the heavy-fermion corrections to the three-loop matching coefficient of the vector current*, Phys. Lett. B **678** (2009) 269 [arXiv:0904.0920 [hep-ph]].

[23] C. Anzai, Y. Kiyo, Y. Sumino, *Static QCD potential at three-loop order*, Phys. Rev. Lett. **104** (2010) 112003 [arXiv:0911.4335 [hep-ph]].

[24] A. V. Smirnov, V. A. Smirnov, M. Steinhauser, *Three-loop static potential*, Phys. Rev. Lett. **104** (2010) 112002 [arXiv:0911.4742 [hep-ph]].

[25] A. H. Hoang, A. V. Manohar, I. W. Stewart, T. Teubner, *A Renormalization group improved calculation of top quark production near threshold*, Phys. Rev. Lett. **86** (2001) 1951 [hep-ph/0011254].

[26] A. A. Penin, A. Pineda, V. A. Smirnov, M. Steinhauser, *Spin dependence of heavy quarkonium production and annihilation rates: Complete next-to-next-to-leading logarithmic result*, Nucl. Phys. B **699** (2004) 183 [hep-ph/0406175].

[27] A. Pineda, A. Signer, *Heavy Quark Pair Production near Threshold with Potential Non-Relativistic QCD*, Nucl. Phys. B **762** (2007) 67 [hep-ph/0607239].

[28] I. I. Y. Bigi, V. S. Fadin, V. A. Khoze, *Stop near threshold*, Nucl. Phys. B **377** (1992) 461.

[29] K. Melnikov, O. I. Yakovlev, *Top near threshold: All α_s corrections are trivial*, Phys. Lett. B **324** (1994) 217 [hep-ph/9302311].

[30] A. A. Penin, A. A. Pivovarov, *Top quark threshold production in $\gamma\gamma$ collision in the next-to-leading order*, Nucl. Phys. B **550** (1999) 375 [hep-ph/9810496].

[31] A. H. Hoang, C. J. Reißer, *Electroweak absorptive parts in NRQCD matching conditions*, Phys. Rev. D **71** (2005) 074022 [hep-ph/0412258].

[32] A. H. Hoang, C. J. Reißer, P. Ruiz-Femenía, *Phase Space Matching and Finite Lifetime Effects for Top-Pair Production Close to Threshold*, Phys. Rev. D **82** (2010) 014005 [arXiv:1002.3223 [hep-ph]].

[33] M. Beneke, B. Jantzen, P. Ruiz-Femenía, *Electroweak non-resonant NLO corrections to $e^+e^- \to W^+W^-b\bar{b}$ in the $t\bar{t}$ resonance region*, Nucl. Phys. B **840** (2010) 186 [arXiv:1004.2188 [hep-ph]].

[34] M. Beneke, A. P. Chapovsky, A. Signer, G. Zanderighi, *Effective theory approach to unstable particle production*, Phys. Rev. Lett. **93** (2004) 011602 [hep-ph/0312331].

[35] W. E. Caswell, G. P. Lepage, *Effective Lagrangians for Bound State Problems in QED, QCD, and Other Field Theories*, Phys. Lett. B **167** (1986) 437.

[36] G. T. Bodwin, E. Braaten, G. P. Lepage, *Rigorous QCD analysis of inclusive annihilation and production of heavy quarkonium*, Phys. Rev. D **51** (1995) 1125 [hep-ph/9407339].

[37] A. Pineda, J. Soto, *Effective field theory for ultrasoft momenta in NRQCD and NRQED*, Nucl. Phys. Proc. Suppl. **64** (1998) 428 [hep-ph/9707481].

[38] N. Brambilla, A. Pineda, J. Soto, A. Vairo, *Potential NRQCD: An Effective theory for heavy quarkonium*, Nucl. Phys. B **566** (2000) 275 [hep-ph/9907240].

[39] M. Beneke, V. A. Smirnov, *Asymptotic expansion of Feynman integrals near threshold*, Nucl. Phys. **B522** (1998) 321 [hep-ph/9711391].

[40] V. A. Smirnov, *Applied asymptotic expansions in momenta and masses*, Springer Tracts Mod. Phys. **177** (2002) 1.

[41] T. Huber and D. Maître, *HypExp 2, expanding hypergeometric functions about half-integer parameters*, Comput. Phys. Commun. **178** (2008) 755 [arXiv:0708.2443 [hep-ph]].

[42] P. Nogueira, *Automatic Feynman graph generation*, J. Comput. Phys. **105** (1993) 279.

[43] R. Harlander, T. Seidensticker, M. Steinhauser, *Complete corrections of $\mathcal{O}(\alpha\alpha_s)$ to the decay of the Z boson into bottom quarks*, Phys. Lett. B **426** (1998) 125 [hep-ph/9712228].

[44] T. Seidensticker, *Automatic application of successive asymptotic expansions of Feynman diagrams*, hep-ph/9905298.

[45] J. A. M. Vermaseren, *New features of FORM*, math-ph/0010025.

[46] M. Jeżabek, J. H. Kühn, *QCD Corrections to Semileptonic Decays of Heavy Quarks*, Nucl. Phys. B **314** (1989) 1.

[47] K. G. Chetyrkin, M. Steinhauser, *Three loop nondiagonal current correlators in QCD and NLO corrections to single top quark production*, Phys. Lett. B **502** (2001) 104 [hep-ph/0012002].

[48] K. Nakamura et al. [Particle Data Group], *Review of particle physics*, J. Phys. G **37** (2010) 075021.

[49] K. G. Chetyrkin, J. H. Kühn, M. Steinhauser, *RunDec: A Mathematica package for running and decoupling of the strong coupling and quark masses*, Comput. Phys. Commun. **133** (2000) 43 [hep-ph/0004189].

[50] S. V. Chekanov, V. L. Morgunov, *Selection and reconstruction of the top quarks in the all hadronic decays at a linear collider*, Phys. Rev. D **67** (2003) 074011 [arXiv:hep-ex/0301014 [hep-ex]].

[51] K. Hagiwara, Y. Sumino, H. Yokoya, *Bound-state Effects on Top Quark Production at Hadron Colliders*, Phys. Lett. B **666** (2008) 71 [arXiv:0804.1014 [hep-ph]].

[52] Y. Kiyo, J. H. Kühn, S. Moch, M. Steinhauser, P. Uwer, *Top-quark pair production near threshold at LHC*, Eur. Phys. J. C **60** (2009) 375 [arXiv:0812.0919 [hep-ph]].

[53] D. Binosi, J. Collins, C. Kaufhold, L. Theussl, *JaxoDraw: A Graphical user interface for drawing Feynman diagrams. Version 2.0 release notes*, Comput. Phys. Commun. **180** (2009) 1709 [arXiv:0811.4113 [hep-ph]].